NASA TECHNICAL NOTE

NASA TN D-8229

NASA TN D-8229

DEGRADATION OF A MULTILAYER INSULATION DUE TO A SEAM AND A PENETRATION

Irving E. Sumner

Lewis Research Center
Cleveland, Ohio 44135

NATIONAL AERONAUTICS AND SPACE ADMINISTRATION • WASHINGTON, D. C. • OCTOBER 1976

1. Report No.	2. Government Accession No.	3. Recipient's Catalog No.
NASA TN D-8229		

4. Title and Subtitle	5. Report Date
DEGRADATION OF A MULTILAYER INSULATION DUE TO A SEAM AND A PENETRATION	October 1976
	6. Performing Organization Code

7. Author(s)	8. Performing Organization Report No.
Irving E. Sumner	E-8622
	10. Work Unit No.
9. Performing Organization Name and Address	506-21
Lewis Research Center National Aeronautics and Space Administration Cleveland, Ohio 44135	11. Contract or Grant No.
	13. Type of Report and Period Covered
12. Sponsoring Agency Name and Address	Technical Note
National Aeronautics and Space Administration Washington, D.C. 20546	14. Sponsoring Agency Code

15. Supplementary Notes

16. Abstract

An experimental investigation was conducted to determine the degradation of the thermal performance of a multilayer insulation due to the presence of a seam and a penetration. The multilayer insulation had 30 aluminized Mylar radiation shields with silk net spacers. The seam, an offset butt joint, caused a heat input of 0.169 watt per meter in addition to the basic insulation thermal performance of 0.388 watt per square meter obtained before the installation of the butt joint. The penetration, a fiberglass tank support strut, provided a heat input (including the degradation of the insulation) of 0.543 watt in addition to the basic insulation thermal performance of 0.452 watt per square meter obtained before the penetration.

17. Key Words (Suggested by Author(s))	18. Distribution Statement
Multilayer insulation; Thermal performance; Cryogenic propellant storage; Spacecraft; Cryogens	Unclassified - unlimited STAR Category 15 (rev.)

19. Security Classif. (of this report)	20. Security Classif. (of this page)	21. No. of Pages	22. Price*
Unclassified	Unclassified	34	$4.00

* For sale by the National Technical Information Service, Springfield, Virginia 22161

DEGRADATION OF A MULTILAYER INSULATION DUE TO A SEAM AND A PENETRATION

by Irving E. Sumner

Lewis Research Center

SUMMARY

An experimental investigation was conducted to determine the degradation of the thermal performance of a multilayer insulation due to the presence of a seam and a penetration. The multilayer insulation consisted of two blankets; each blanket contained 15 double-aluminized Mylar radiation shields alternated with 16 double silk net spacers. The radiation shields and silk net spacers of each blanket were enclosed between two laminated, aluminized Mylar/Dacron scrim cover sheets. The seam configuration consisted of a butt joint in each insulation blanket that was offset by 8.9 centimeters (3.5 in.). A cylindrical fiberglass tank-support strut that penetrated the insulation was installed for the penetration test.

The multilayer insulation blankets tested were flat circular panels 147 centimeters (58 in.) in diameter. The thermal performance was experimentally determined by means of a flat-plate calorimeter. All insulation thermal performance tests were conducted under vacuum conditions at a nominal hot-boundary temperature of 300 K (540° R) with liquid hydrogen as the heat sink.

The experimental results indicated that the presence of the particular seam configuration tested caused a heat input of 0.169 watt per meter (0.176 Btu/hr-ft) along the length of the seam, in addition to the basic multilayer insulation thermal performance of 0.388 watt per square meter (0.123 Btu/hr-ft^2) obtained before the installation of the seam. The presence of the fiberglass strut penetrating the multilayer insulation blankets caused a gradient in the radial temperature profile of the insulation out to a radius of approximately 50 centimeters (20 in.) and provided a heat input of 0.543 watt (1.853 Btu/hr) in addition to the basic multilayer insulation thermal performance of 0.452 watt per square meter (0.143 Btu/hr-ft^2) obtained before the installation of the strut.

INTRODUCTION

The advent of high-energy upper-stage space vehicles and long orbital and planetary missions has led to the development of multilayer insulation (MLI) for use in cryogenic storage. Investigations (e.g., refs. 1 to 3) have shown that MLI can be effective in reducing radiant heat transfer to cryogenic propellant tanks, which for long missions can be the major mode of heat transfer.

To examine some of the problems associated with the design, fabrication, installation, and testing of a thermal protection system for a prototype high-energy upper stage, the Lewis Research Center started work on a cryogenic storage test vehicle (CSTV) in the early 1970's. The CSTV used shadow shields in conjunction with a payload-toward-the-Sun orientation for deep-space thermal protection and a modularized 30-layer, tank-mounted, multilayer insulation system for thermal protection while in a near-Earth environment. This insulation system consisted of twelve 60°-gore panels mounted on the side of the liquid-hydrogen propellant tank and four conical polar caps located at the top and bottom of the tank. The liquid-hydrogen propellant tank, surrounding truss structure, shadow shields, and simulated payload were subsequently tested in both the deep-space and near-Earth environments (refs. 4 to 6). To determine more precisely the basic thermal performance of the CSTV tank-mounted multilayer insulation system for the near-Earth environmental conditions, it was desirable to conduct separate subscale thermal performance tests to determine the effect of (1) the seams between the MLI 60°-gore panels and (2) the penetrations through the insulation panels.

The CSTV multilayer insulation system itself was composed of two insulation blankets, each consisting of 15 double-aluminized Mylar radiation shields alternated with 16 double silk net spacers. The radiation shields and silk net spacers of each blanket were enclosed between two laminated aluminized Mylar/Dacron scrim cover sheets. The edges of two adjacent MLI 60°-gore panels were butted to form a butt joint with a portion of the cover sheet overlapping the butt joint on each side of the insulation blankets. The butt joints in the inner and outer insulation blankets were offset to further insure that there was no direct path for thermal radiation to reach the propellant tank. The major penetrations through the insulation panels were 12 fiberglass tank support struts. To accommodate the modularized insulation concept, the insulation panels were notched in the area of the tank support brackets to allow for easy removal and replacement of the insulation panels. The notched areas where the fiberglass struts were attached to the tank support brackets were covered with a five-layer MLI panel.

The purpose of this report is to present the results of Lewis investigation to experimentally determine the degradation in thermal performance of the basic MLI of the CSTV tank-mounted insulation system caused by the presence of (1) the seams in the MLI blankets and (2) a fiberglass tank support strut penetrating the insulation. The MLI panels tested were flat, circular panels, 147 centimeters (58 in.) in diameter. The

thermal performance of the MLI was experimentally determined with a double-guarded flat-plate calorimeter that was 152 centimeters (60 in.) in diameter. The tests were conducted at a nominal hot-boundary temperature of 300 K (540° R) with liquid hydrogen as the low-temperature heat sink. With one exception, the tests were conducted in a vacuum of 1×10^{-4} newtons per square meter (1×10^{-6} torr) or less to reduce the heat transfer due to gaseous conduction within the insulation.

SYMBOLS

d depth of gap in butt joint, m (ft)

f dimensionless function of butt joint width to depth ratio, δ/d

K thermal conductivity, W/m·K (Btu/hr-ft-°R)

ℓ length of butt joint, m (ft)

N number of radiation shields

$\bar{N}$ layer density, layers/cm (layers/in.)

P interstitial pressure, N/m^2 (torr)

Q heat flux, W/m^2 ($Btu/hr-ft^2$)

q heat-transfer rate, W (Btu/hr)

r radius, m (ft)

T temperature, K (°R)

t thickness of aluminizing per radiation shield, m (ft)

δ width of gap in butt joint, m (ft)

ϵ room-temperature emissivity of aluminized surfaces of radiation shields

ρ_n near-normal reflectivity of aluminized surfaces of radiation shields

σ Stefan-Boltzmann constant, 5.670×10^{-8} $W/m^2\ K^4$ (1.714×10^{-9} $Btu/hr-ft^2-{}^oR^4$)

Subscripts:

av average

bj butt joint

c cold

h hot

i i^{th} component

l	lateral input
m	aluminizing on radiation shields
meas	measured input
net	net input
null	null input
p	predicted
s	strut
tot h	total hemispherical
tot n	total normal
1	inner radial location
2	outer radial location

EXPERIMENTAL APPARATUS

Calorimeter

All of the multilayer insulation thermal performance tests were conducted on a large, flat-plate calorimeter (figs. 1 and 2). The MLI thermal performance was determined by measuring the heat input (liquid-hydrogen boiloff) into the measure tank. The 112-centimeter (44-in.) diameter measure tank was filled with copper wool to prevent temperature stratification of the liquid hydrogen. The measure tank was set into an inner and outer cold guard (fig. 1), each of which was 147 centimeters (58.0 in.) in diameter. The cold guards reduced extraneous heat leaks into the measure tank and minimized insulation edge effects on the heat-transfer measurements. Cold traps were provided on the vent and fill lines for the measure tank to reduce the extraneous heat leaks into the measure tank from this source. The two cold traps were continually filled with liquid hydrogen from the outer cold guard and were vented to the ullage volume of the inner cold guard.

A socket in the center of the measure tank was provided so that a thermal link could be mechanically attached to the measure tank. The thermal link provided a separate measurement of the heat input to the measure tank coming from the fiberglass strut that was penetrating the multilayer insulation.

The three tanks were constructed of oxygen-free, high-conductivity (OFHC) copper having a minimum thickness of 0.95 centimeter (3/8 in.) to minimize the temperature gradients in the tank walls. The tanks were supported and thermally isolated from each other by small Bakelite spacers.

The hot-side boundary temperature for the multilayer insulation was maintained by the shroud assembly. The outer shroud could be chilled to cryogenic temperatures by flowing liquid nitrogen or liquid hydrogen through cooling coils welded to the top and sides of the shroud. The liquid-hydrogen boundary temperature was required when conducting a null test to determine the extraneous heat leaks into the measure tank. The inner shroud assembly, consisting of three separate heating zones, was used to provide the desired hot-side boundary temperature for the insulation thermal performance tests. The temperature of each heating zone, which was maintained by a separate electrical heater, could be set at any desired boundary temperature between 78 and 389 K (140° and 700° R). Except during a null test, the hot-side boundary temperature was set at 300 K (540° R) for this test program.

The flat, circular multilayer insulation blankets were mounted on the top of the measure tank and inner cold guard for the thermal performance tests. Thus, the only force tending to compress the insulation blankets was the weight of the blankets themselves. The width (17.3 cm (6.8 in.)) of the inner cold guard as well as the heated edge guard minimized the effect of any radial temperature gradients present near the edge of the MLI blankets. The edge guard was fabricated from 0.16-centimeter (1/16-in.) thick Teflon, etched for adhesive bonding. The Teflon strip was both adhesively bonded and mechanically fastened to the edge of the inner cold guard. The top of the edge guard was heated by a Nichrome alloy wire; the temperature at the bottom was maintained close to liquid-hydrogen temperature by the inner cold guard to approximate the normal temperature profile through the multilayer insulation. The inside surface of the edge guard was covered with aluminized Mylar tape to minimize radiation heat transfer (radiation tunnelling) laterally into the multilayer insulation. The temperature profile from the top to the bottom of the edge guard was monitored by several Chromel-Constantan thermocouples. The electrical power to the Nichrome heater was adjusted to maintain the temperature of the top of the edge guard to approximately 300 ± 11 K ($540^{\circ}\pm20^{\circ}$ R).

A view of the calorimeter ready for installation and inspection of the multilayer insulation system is shown in figure 2. A second view of the calorimeter, with additional insulation added to the bottom and sides and ready for installation in the vacuum chamber, is shown in figure 3. The additional insulation was required to prevent the cryogenic liquid in the outer cold guard and cold traps from boiling away too rapidly.

Vacuum Chamber

All tests were conducted with the calorimeter mounted within a cylindrical vacuum chamber 1.83 meters (72 in.) in diameter by 2.90 meters (114 in.) high. Three 0.25-meter (10-in.) oil diffusion pumps were provided a vacuum capability in the high 10^{-4} newton per square meter (10^{-6} torr) range at ambient temperature and in the low 10^{-4}

newton per square meter (10^{-6} torr) or high 10^{-5} newton per square meter (10^{-7} torr) range with the calorimeter filled with liquid hydrogen.

Multilayer Insulation

Two separate sets of multilayer insulation blankets were used in this test program. The first set was used to experimentally determine the thermal degradation caused by the presence of a seam in the insulation blankets; the second set was used to determine the degradation caused by the presence of a fiberglass tank-support strut penetrating the insulation blankets. In each case the MLI blankets were tested, first, to determine the basic thermal performance of the undisturbed insulation and then, second, to determine the thermal performance after the insulation had been modified to incorporate the seam or penetration.

The basic multilayer insulation used for each thermal performance test consisted of two MLI blankets. Each blanket consisted of 15 double-aluminized Mylar radiation shields alternately spaced with 16 double silk net spacers. A laminated, aluminized Mylar/Dacron scrim cover sheet was applied to each side of each blanket. The layup of cover sheets, radiation shields, and silk net spacers was held together by nylon button-pin studs spaced on 20-centimeter (8-in.) centers. Each MLI blanket was 147 centimeters (58.0 in.) in diameter. The first two-blanket MLI configuration tested in this program had a nominal measured layer density of 17.4 layers per centimeter (44.2 layers/in.), and the second two-blanket configuration had a nominal measured layer density of 20.6 layers per centimeter (52.3 layers/in.). The difference was caused by the layup of the silk net spacers and the length of the nylon button-pin studs used in assemblying the MLI blankets.

After the first two-blanket MLI configuration had been tested for this program to determine its basic thermal performance, the blankets were modified to create a butt joint between the two segments of each blanket as shown in figure 4. The butt joint in each blanket was overlapped by the cover sheet on each side to prevent thermal radiation from penetrating directly through the blanket. The width of the gap between the two segments of each blanket was nominally maintained at approximately 0.3 centimeter (1/8 in.). The offset between the butt joints in the first and second MLI blankets was 8.9 centimeters (3.5 in.). Velcro fasteners adhesively bonded to the face of the calorimeter and the cover sheets maintained the width of the gap and the offset of the butt joints during the thermal performance test. A photograph of the MLI blankets with the butt joint, as installed on the calorimeter, is shown in figure 5.

After the second two-blanket MLI configuration had been tested to determine its basic thermal performance, the blankets were modified to allow penetration of the fiberglass tank-support strut. A photograph of the strut, installed on the face of the calorimeter

without the MLI blankets, is shown in figure 6. This strut was identical to the ones used to support the CSTV liquid-hydrogen tank from its truss structure. The hollow fiberglass (ref. 7) strut had a nominal outside diameter of 3.81 centimeters (1.50 in.) and a nominal wall thickness of 0.076 centimeter (0.030 in.). The length of the strut was 66 centimeters (26 in.) from center to center of the end fittings. The hollow interior of the strut was approximately half filled with chopped aluminized Mylar/Dexiglas to act as a thermal radiation barrier. As shown in figure 6, the strut was attached to an aluminum model of the CSTV tank support bracket. The bracket, in turn, was adhesively bonded and mechanically fastened to the thermal link which was threaded into the socket in the center of the measure tank. Small rectangular holes were cut through the MLI blankets to allow the attachment point of the support bracket to penetrate the insulation. The attachment point where the fiberglass strut was bolted to the tank support bracket and the adjacent area were covered with a five-layer blanket, which was attached to the outer main insulation blanket with Velcro fasteners. The outer cover sheet of the five-layer MLI blanket ran part way up the strut (fig. 7) and was then taped in place.

Instrumentation and Controls

The radial and normal temperature profiles for the MLI blankets were measured with 0.020-centimeter (0.008-in.) diameter wire Chromel-Constantan thermocouples. The radial thermocouple pattern used on the six instrumented radiation shields (shields 1, 9, 17, 18, 26, and 34 starting from the coldest shield adjacent to the measure tank and inner cold guard) for the first MLI blanket configuration is shown in figure 4. The radial thermocouple patterns used on the 10 instrumented radiation shields (shields 1, 5, 9, 13, 17, 18, 22, 26, 30, and 34) for the second MLI blanket configuration used with the fiberglass tank support strut is shown in figure 8. The thermocouple junctions as well as the constant-radius isothermal lead lengths of the wires were adhesively bonded to either a cover sheet or radiation shield and then covered completely with aluminized Mylar tape. The thermocouple wires were then run radially to the edge of the sheet and shield and were continuously taped in place. Thermocouples of the same type were also attached in a similar manner to the fiberglass tank-support strut. Additional Chromel-Constantan thermocouples were also used to measure temperatures of the calorimeter tanks, cryogenic service lines, and shroud assembly. The temperatures measured by the Chromel-Constantan thermocouples had a maximum uncertainty ($3\text{-}\sigma$ deviation) of ± 5 K ($\pm 9^{\circ}$ R) at liquid-hydrogen temperature. This uncertainty improved to ± 2.33 K ($\pm 4.2^{\circ}$ R) at room temperature.

Additional temperature measurements at certain points on the calorimeter tanks, cryogenic service lines, and the inner shroud assembly were obtained using platinum resistance thermometers to improve the accuracy of the measurements. These

thermometers had a maximum uncertainty (3-σ deviation) of ±0.09 K (±0.16° R) at liquid-hydrogen temperature and ±0.4 K (±0.7° R) at the normal shroud temperature of 300 K (540° R).

Measure tank and cold-guard pressures were measured with bonded strain gage transducers which had an estimated uncertainty of ±0.25 percent of full scale. Vacuum levels within the vacuum chamber were measured by means of ionization gages.

The measure-tank and cold-guard pressures were maintained at a constant level by separate closed-loop control systems as shown in figure 9. These pressure-control systems used high-resolution, differential-pressure, capacitance transducers which sensed very small pressure variations inside the tanks relative to an absolute reference pressure. The electrical output signals from the transducers were transmitted to control units for the motorized pressure-regulating valves in the measure tank and cold-guard vent lines in order to regulate the liquid-hydrogen boiloff flow rates, thereby maintaining the tank pressures at constant values. The reference pressure was provided by a 0.0148 cubic meter (0.523 ft^3) gaseous nitrogen tank maintained at a constant temperature by an ice bath. This system maintained the measure tank and cold-guard pressures to within 5.5 newton per square meter (0.0008 psi) of the desired value. The desired measure tank pressure was varied slightly from test to test within the range of 1.00×10^5 to 1.43×10^5 newton per square meter (14.5 to 16.6 psia). It was not necessary to closely control the cold-guard pressure to a narrow ΔP band slightly above the measure tank pressure for this flat-plate calorimeter configuration because the measure tank was located above the cold-guard tanks. However, the cold-guard pressure was controlled between 70 and 140 newtons per square meter (0.01 and 0.02 psi) above the measure tank pressure during approximately one-half of the tests conducted.

The liquid-hydrogen boiloff flow rate from the measure tank was metered by one of four mass flowmeters. These meters were calibrated with gaseous hydrogen and had nominal full-scale ranges of 0 to 10, 0 to 50, 0 to 500, and 0 to 5000 standard cubic centimeters per minute (0.021, 0.106, 1.06, and 10.6 scfh). The uncertainty associated with these meters was ±0.5 percent of full scale.

The temperature of the inner shroud assembly was controlled in a closed-loop mode by three separate direct-current electrical heaters and their associated controllers. The temperature of the inner shroud assembly was maintained at 300±1 K (540°±2° R) except during the null tests.

A thermal link was used to determine the heat input from the penetration to the measure tank separately. The thermal link consisted of a thin top plate, 10 centimeters (4 in.) in diameter, and a cylindrical shaft, 10.8 centimeters ($4\frac{1}{4}$ in.) long and 1.42 centimeters (0.560 in.) in diameter, machined from phosphorus deoxidized copper. The shaft was threaded to mate with the socket in the center of the measure tank. The temperature difference between the top and the bottom of the cylindrical shaft, as measured

by two platinum resistance thermometers, was used as an indication of the heat transfer through the thermal link. An electrical calibration of the thermal link was conducted during the basic thermal performance test of the second two-blanket MLI configuration by means of a direct-current electrical heater adhesively bonded to the top of the thermal link. The result of the electrical calibration is shown in figure 10.

All measurements were recorded on a high-speed digital data system.

TEST PROCEDURE

Insulation Thermal Performance Tests

For a typical experimental run, the vacuum chamber was initially pumped down to less than 1×10^{-2} newton per square meter (1×10^{-4} torr) vacuum level and then backfilled with gaseous helium to 30 newtons per square meter (2×10^{-1} torr). This procedure was repeated three times to insure a helium background in the vacuum chamber and insulation blankets. The vacuum chamber was then evacuated to the low 10^{-3} newton per square meter (10^{-5} torr) range and held at that level for at least 48 hours to remove the interstitial gases from within the MLI blankets. The inner shroud assembly, closed-loop temperature controllers were then turned on as well as the edge guard heater. The cold guards and measure tank were then filled with liquid hydrogen and allowed to vent directly to the atmosphere. A several hour chilldown followed, during which the MLI temperatures approached their steady-state values and the liquid-hydrogen boiloff rate approach 5000 standard cubic centimeters per minute (10.6 scfh), which was the upper limit that could be measured by the largest of the mass flowmeters. The tanks were retopped with liquid hydrogen as required.

The pressure in the measure tank and cold guards was then brought under control by the closed-loop pressure-control system. Temperature stratification of the liquid hydrogen in the measure tank was minimized by the copper wool and copper structural posts within the measure tank. The liquid-hydrogen boiloff rate continued to decrease to a steady-state value. Thermal equilibrium conditions were assumed to have been reached when the MLI temperatures changed less than 0.6 K (1° R) over a 1-hour period and when the boiloff rate was within a ±2 percent of a given value over a 4-hour period.

Null Tests

The null tests were conducted with the electrical power to all electrical heaters turned off and with liquid hydrogen circulating through the outer shroud. The vacuum chamber was backfilled with gaseous helium to 30 newtons per square meter

(2×10^{-1} torr) for a short time to increase the chilldown rate of the MLI blankets and the inner shroud assembly. The chamber was then evacuated again, and the test was continued with all temperatures at or somewhat above liquid-hydrogen temperature until a steady-state boiloff rate was obtained.

HEAT TRANSFER EQUATIONS

The normal heat flux through each set of MLI blankets was predicted using the following equation obtained from reference 1:

$$Q_p = \frac{8.95\times10^{-8}(\bar{N})^{2.56}}{N-1}\left(\frac{T_h^2 - T_c^2}{2}\right) + \frac{5.39\times10^{-10}\,\epsilon_{tot\ h}}{N-1}\left(T_h^{4.67} - T_c^{4.67}\right) + \frac{3.67\times10^{2}\,P}{N-1}\left(T_h^{0.26} - T_c^{0.26}\right) \quad (1)$$

In equation (1) the first term represents the solid conduction heat-transfer component, the second term represents the radiation component, and the third term represents the gaseous conduction component. The layer density $\bar{N}$ was the average value determined from thickness measurements of each of the MLI blankets. The hot and cold boundary temperatures (T_h and T_c) used were the measured temperatures of the warmest and coldest cover sheet of the MLI blanket configuration. The predicted heat flux Q_p was calculated assuming that the two-blanket MLI configuration acted as one continuous MLI blanket so that the heat transfer between the two adjacent cover sheets (radiation shields 17 and 18) could be treated in the same manner as any two radiation shields with a double silk net spacer between them. The room temperature emissivity $\epsilon_{tot\ h}$ of the radiation shields was the average value of total hemispherical emittance as determined by a Gier Dunkle reflectometer, model DB 100. The reflectometer provides a measurement of the near-normal reflectance ρ_n of the surface of a sample. The total hemispherical emittance $\epsilon_{tot\ h}$ of the radiation shields was then calculated from the following equation as suggested by reference 1:

$$\epsilon_{tot\ h} = 1.33\,\epsilon_{tot\ n} = 1.33(1 - \rho_n) \quad (2)$$

The value of the interstitial pressure P used to calculate the predicted heat flux was assumed to be the measured vacuum chamber pressure.

It was necessary to make a correction to the measured heat input to the measure tank due to any radial temperature gradients that might exist because of edge effects in the MLI blankets. The lateral (or radial) heat input was calculated on the basis of the measured MLI temperature profiles at radii of 53.3 and 58.4 centimeters (21.0 and 23.0 in.) from the center of the measure tank (see figs. 4 and 8). The lateral heat input for all radiation shields and cover sheets was calculated from

$$q_l = \sum_{i=1}^{N} \frac{2\pi(K_m)_i \, t(T_2 - T_1)_i}{\ln (r_2/r_1)} \tag{3}$$

where $t = 8\times10^{-8}$ meter (2.63×10^{-7} ft), $r_2/r_1 = 1.095$, and $N = 34$.

There is some uncertainty in the magnitude of the calculated values of the lateral heat input due to (1) the small differences in the measured values of the radiation shield temperature T_1 and T_2 and (2) the interpolation required to obtain shield temperatures of the radiation shields between those on which the temperatures were actually measured. In general, however, the calculated lateral heat input was small compared with the measured heat input for each test and, therefore, should not create any large uncertainty in the corrected (or net) heat input to the measure tank.

The thermal conductivity K_m of the thin aluminum film deposited on the radiation shields and cover sheets was calculated from the following equation derived from information presented in reference 8:

$$K_m = 102.4 + 0.2423\left(\frac{T_1 + T_2}{2}\right) \tag{4}$$

The contribution of radiation tunnelling and the Mylar to the overall effective lateral thermal conductivity of the aluminized Mylar radiation shields and cover sheets was considered small, and was therefore neglected.

The net heat input into the measure tank, which represented the actual thermal performance of the multilayer insulation (and seam or fiberglass strut, if present), was calculated from the following equation:

$$q_{net} = q_{meas} - q_l - q_{null} \tag{5}$$

The thermal conductivity K_s of the fiberglass strut was calculated from the following equation obtained from information presented in reference 7:

$$K_s = 6.793\times10^{-2} + 2.856\times10^{-3}\, T_{av} - 4.541\times10^{-6}\, T_{av}^2 - 1.079\times10^{-10}\, T_{av}^3 \qquad (6)$$

where T_{av} is the average of wall temperatures measured 2.5 and 5.1 centimeters (1 and 2 in.) from the cold end of the strut.

RESULTS AND DISCUSSION

Thermal Performance of Multilayer Insulation with Butt Joint

The basic thermal performance of the first MLI two-blanket configuration without the butt joint was determined first. A summary of the measured thermal performance is shown in table I (test 2). The experimentally determined heat input into the measure tank of the calorimeter was 0.373 watt (1.275 Btu/hr). This value was then corrected for both the lateral heat input due to radial temperature gradients in the MLI test specimen and the null heat input (test 1, unpublished data obtained in a previous test program). The negative value of the lateral heat input (table 1) calculated from the existing radial temperature gradient for test 2 indicated that the net lateral heat flow was radially outward (away from the measure tank) rather than inward. The resulting normal net heat input was 0.381 watt (1.301 Btu/hr) or a normal net heat flux of 0.388 watt per square meter (0.123 Btu/hr-ft^2).

The predicted heat flux Q_p calculated for the test conditions existing during test 2 was 0.387 watt per square meter (0.123 Btu/hr-ft^2) as noted in table II. The measured net heat flux was within approximately 0.3 percent of the predicted heat flux. The magnitude of the solid conduction, radiation, and gaseous conduction heat-transfer components are also noted in table II. The radiation component was calculated to be slightly greater than the solid conduction component, while the contribution of the gaseous conduction component was very small.

The radial and normal temperature profiles measured during test 2 are shown in figure 11. Shields 1, 17, 18, and 34 represent the cover sheets of the two MLI blankets. Most of the MLI radiation shields showed little radial temperature gradient existing over the measure tank (fig. 11(a)) except for the first (coldest) cover sheet and perhaps the first few radiation shields.

The experimentally determined normal temperature profile (fig. 11(b)) represents average values of the MLI shield temperatures obtained near the center of the test specimen. The experimental data are compared with a predicted temperature profile calculated from equation (1) using the experimentally measured vacuum-chamber pressure as the interstitial pressure P and using the predicted heat flux Q_p. The predicted temperature profile was calculated continuously through the two-blanket MLI configura-

tion assuming that the heat transfer between the two adjacent cover sheets (radiation shields 17 and 18) could be treated in the same manner as any two radiation shields with a double silk net spacer between. A very good agreement was obtained between the measured and predicted normal temperature profiles throughout both MLI blankets for the first MLI blanket configuration.

The thermal performance of the first MLI two-blanket configuration with the butt joint incorporated in the blankets is shown in table I (test 3). The measured heat input was 0.584 watt (1.995 Btu/hr), and the net heat input was calculated to be 0.570 watt (1.947 Btu/hr). The difference in the values of the corrected heat input between test 2 and 3 indicates that the degradation in thermal performance due to the butt joint was 0.189 watt (0.646 Btu/hr) or 0.169 watt per meter (0.176 Btu/hr-ft) along the length of the butt joint. The average value was about 0.30 watt per meter (0.32 Btu/hr-ft) that would be predicted for an assumed gap width of about 0.318 centimeter (0.125 in.) from the following equation obtained from reference 9:

$$\frac{q}{l_{bj}} = df\sigma\left(T_h^4 - T_c^4\right) \tag{7}$$

The radial temperature profiles measured during test 3 are shown in figure 12. Some disturbance to the normal radial temperature profiles can be noted for the inner cover sheet (shield 1) and probably the first few radiation shields. Otherwise, no significant differences were noted in the radial temperature profiles between tests 2 and 3.

Thermal Performance of Multilayer Insulation with Penetration

The basic thermal performance of the second MLI two-blanket configuration is shown in table I (test 4). The experimentally determined heat input into the measure tank was 0.473 watt (1.615 Btu/hr). The corrected normal net heat input was 0.443 watt (1.513 Btu/hr), or a normal net heat flux of 0.452 watt per square meter (0.143 Btu/hr-ft^2). The predicted heat flux for this blanket configuration was calculated to be 0.494 watt per square meter (0.157 Btu/hr-ft^2) as noted in table II. The net measured heat flux was within 8.5 percent of the predicted heat flux. Because of the slightly higher layer density of the second MLI blanket, the solid conduction heat-transfer component (1) had increased from that calculated for the first MLI blanket configuration (test 2) and (2) was greater than the radiation component calculated for test 4.

The radial and normal temperature profiles measured during test 4 are shown in figure 13. The radial temperature profiles noted for this test are very similar to those noted previously for the first MLI two-blanket configuration (fig. 11(a)), although the slight difference was sufficient to change the correction for the lateral heat input from

radially outward to radially inward. The measured normal temperature profile agreed fairly well with the predicted normal temperature profile (fig. 13(b)) for the assumed interstitial pressure of 1.7×10^{-4} newton per square meter (1.3×10^{-6} torr) and the predicted heat flux of 0.494 watt per square meter (0.157 Btu/hr-ft^2).

The overall thermal performance of the second MLI two-blanket configuration modified to allow the penetration of the tank support bracket and fiberglass strut is shown in table I (test 5). The measured heat input was 1.260 watts (4.302 Btu/hr), and the net heat input was calculated to be 0.986 watt (3.366 Btu/hr). It should be noted that a subsequent null test (test 7) indicated that the null heat input had increased to 0.235 watt (0.801 Btu/hr). Of this value, 0.149 watt (0.508 Btu/hr) (test 8) was attributed to the failure of an adhesive bond on the inner cold guard (fig. 14), thermally shorting eight 26-gage copper instrument-lead wires for measure tank temperature measurements as well as the previous miscellaneous heat inputs (test 1). The remaining 0.086 watt (0.293 Btu/hr) (the difference between tests 7 and 8) was attributed to ten 24- and 26-gage copper instrument-lead wires for the thermal link, which were thermally shorted to the inner cold guard by means of double-stick and aluminized Mylar tape. These adhesive bonds apparently remained intact through test 4. This was at least partially confirmed by visual inspection performed when the second MLI two-blanket configuration was removed from the calorimeter for modification. It is believed that the adhesive bonds failed when the calorimeter was chilled down for test 5.

The radial temperature gradients existing in the MLI blankets for test 5 are shown in figure 15. The radial gradients in the plane of the axis of the fiberglass strut are shown in figure 15(a) and normal to the plane of the strut in figure 15(b). Fairly significant radial temperature gradients out to a radius of approximately 50 centimeters (20 in.) can be noted directly underneath the end fitting of the strut where the MLI was slightly compressed and to each side of the tank support bracket. These gradients would lead to some heat transfer laterally along the radiation shields to the tank support bracket.

The temperature gradient along the fiberglass strut for test 5 is shown in figure 16. The data indicate that ambient temperature was maintained along the strut to about 20 centimeters (8 in.) from the cold end of the strut. The cold end temperature of 158 K (284° R) on the strut was achieved without imposing any significant tensile load on the strut. This would be representative of the zero gravity coast phase of a space vehicle where it is in a weightless condition.

The presence of the tank support bracket and fiberglass strut increased the net heat input through the second MLI two-blanket configuration by 0.543 watt (1.854 Btu/hr). A summary of the breakdown of the overall heat input components is noted in table III and is also pictured in the following sketch:

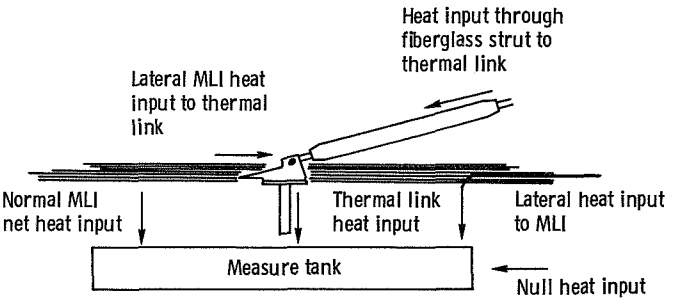

The total heat input through the thermal link was determined to be 0.446 watt (1.522 Btu/hr). Of that total, the heat conduction along the strut was calculated to be 0.140 watt (0.478 Btu/hr). The remaining heat input through the thermal link can be attributed to the lateral heat flow along the radiation shields and cover sheets in the vicinity of the tank support bracket for the strut; this heat input is then 0.306 watt (1.044 Btu/hr). The portion of the net heat input not conducted through the thermal link must be attributed to the normal net heat input through multilayer insulation; this value is then 0.540 watt (1.844 Btu/hr). The total heat input that can then be attributed to the MLI (normal plus lateral heat flow to the thermal link) is then 0.846 watt (2.888 Btu/hr)). Since the previously measured heat input through the MLI without the penetration (test 4) was 0.443 watt (1.513 Btu/hr), the degradation in the thermal performance of the MLI due to the presence of the penetration was 0.403 watt (1.376 Btu/hr).

Some possibility exists that the null heat input correction of 0.020 watt (0.070 Btu/hr) used for test 4 (table I) could also apply to test 5 rather than the value of 0.235 watt (0.801 Btu/hr) that was used. For this case the net heat input into the measure tank would have been 1.201 watts (4.101 Btu/hr), and the degradation in the thermal performance of the MLI due to the presence of the penetration would have been 0.618 watt (2.110 Btu/hr). The difference between 0.403 and 0.618 watt (1.376 and 2.110 Btu/hr) represents a potential range of values that could be assigned to the degradation of the MLI thermal performance. On the basis of visual observation of the copper electrical leads thermally shorted to the inner cold guard before test 5, the value of 0.403 watt (1.376 Btu/hr) is believed to be the more correct value for degradation of the MLI thermal performance due to the presence of the fiberglass strut.

A second thermal performance test with the fiberglass strut penetrating the two blankets of MLI was conducted with the vacuum level in the vacuum chamber increased to approximately 6.4×10^{-2} newton per square meter (4.8×10^{-4} torr) by bleeding in gaseous helium. This test was conducted to duplicate a similar test condition imposed on the CSTV. The thermal performance of the insulation at this vacuum level is noted in tables I, II, and III (test 6). The measured heat input was 2.410 watts (8.228 Btu/hr), and the net heat input was calculated to be 2.103 watts (7.180 Btu/hr). The predicted heat flux for undisturbed (i.e., not disturbed by the presence of a penetration in the vi-

cinity) multilayer insulation at this vacuum level is 1.938 watts per square meter (0.615 Btu/hr-ft^2) as noted in table II. The gaseous conduction component accounts for approximately 75 percent of the total predicted heat flux.

The radial temperature profile for the multilayer insulation (test 6) is shown in figure 17(a). The general decrease in radiation shield temperatures in the vicinity of the tank support bracket for the fiberglass strut is similar to that noted at the lower vacuum level (test 5). The normal temperature profile of the insulation is shown in figure 17(b). The experimental temperatures shown are the average temperatures measured at a radial distance of 53.3 centimeters (21.0 in.) from the center of the insulation. Although these temperatures may have been slightly influenced by the presence of the penetration or the edge guard, they appear to be fairly representative of the undisturbed temperature profile. The predicted temperature profile was obtained from equation (1) using the predicted heat flux of 1.938 watts per square meter (0.615 Btu/hr-ft^2). The predicted normal temperature profile is somewhat lower than the measured temperature profile. The temperature profile along the fiberglass strut (fig. 18), was very similar to that obtained in the previous test. The heat inputs calculated for the thermal link and fiberglass strut along with those attributed to the lateral and normal heat flow through the multilayer insulation are noted in table III. Since the predicted, undisturbed MLI heat input was 1.902 watts (6.494 Btu/hr) and the heat input attributed to the fiberglass strut was 0.145 watt (0.495 Btu/hr), the calculated thermal performance degradation of the MLI blankets in the vicinity of the strut was 0.056 watt (0.191 Btu/hr).

The last tests conducted were two additional null tests to determine if the value of the null heat leak into the measure tank (test 1) had changed during the course of the test program. These null tests (tests 7 and 8) were conducted with the second, two-blanket multilayer insulation configuration and with fiberglass strut still mounted on the calorimeter. This, however, did not influence the test results as the insulation and strut temperatures were all reasonably close (within 22 K (40° R)) of liquid-hydrogen temperature. The total predicted heat input through the undisturbed MLI blankets would have been only about 0.005 watt (0.017 Btu/hr) as noted in table II for test 7. Temperature measurements along the thermal link indicated that there was no heat flow along the link from the fiberglass strut. These null tests (tests 7 and 8, tables I and II) indicated that the null heat input had increased to 0.235 watt (0.801 Btu/hr) as discussed previously.

SUMMARY OF RESULTS

An experimental investigation was conducted to determine the degradation in the thermal performance of a multilayer insulation due to the presence of a seam and a penetration. The multilayer insulation, which was basically the same as that tested previously on a cryogenic storage test vehicle at Lewis, consisted of two blankets of insula-

tion. Each blanket contained 15 double-aluminized Mylar radiation shields alternated with 16 double silk net spacers. The radiation shields and silk net spacers for each blanket were enclosed between two laminated aluminized Mylar/Dacron scrim cover sheets. The seam configuration consisted of a butt joint in each insulation blanket that was offset by 8.9 centimeters (3.5 in.). The penetration configuration was a cylindrical fiberglass tank support strut identical to the ones used with the cryogenic storage test vehicle.

The flat, circular insulation blankets were tested on a flat-plate calorimeter 152 centimeters (60 in.) in diameter. All insulation thermal performance tests were conducted under vacuum conditions at a nominal hot-boundary temperature of 300 K (540° R) with liquid hydrogen as the heat sink.

The following experimental test results were obtained:

1. The basic thermal performance of the undisturbed MLI blankets was 0.388 and 0.452 watt per square meter (0.123 and 0.143 Btu/hr-ft^2) for the two sets of MLI blankets tested. These two experimental values were within 8.5 percent of the predicted values obtained from the semiempirical equation presented in reference 1 using the measured vacuum chamber pressure as the multilayer insulation interstitial pressure.

2. The offset butt-joint configuration tested provided an additional heat input of 0.169 watt per meter (0.176 Btu/hr-ft) along the length of the seam. This was somewhat less than the predicted degradation of 0.30 watt per meter (0.32 Btu/hr-ft).

3. The presence of the fiberglass strut penetrating the MLI blankets caused (1) a disturbance in the radial temperature profile of the MLI out to a radius of approximately 50 centimeters (20 in.) and (2) an additional net heat input of 0.543 watt (1.854 Btu/hr). Of this value, 0.140 watt (0.478 Btu/hr) of heat input could be attributed directly to heat conduction along the fiberglass strut. The actual degradation in the thermal performance of the MLI due to the presence of the penetration was then 0.403 watt (1.376 Btu/hr).

4. The thermal performance test of the MLI blankets with the fiberglass strut at a vacuum level of 6.4×10^{-2} newton per square meter (4.8×10^{-4} torr) indicated a total heat input of 2.103 watts (7.180 Btu/hr). Because the predicted, undisturbed MLI heat input was 1.902 watts (6.494 Btu/hr) and the heat input attributed to the fiberglass strut was 0.145 watt (0.495 Btu/hr), the calculated thermal performance degradation of the MLI blankets in the vicinity of the strut was 0.056 watt (0.191 Btu/hr).

Lewis Research Center,
National Aeronautics and Space Administration,
Cleveland, Ohio, March 3, 1976,
506-21.

REFERENCES

1. Keller, C. W.; Cunnington, G. R.; and Glassford, A. P.: Thermal Performance of Multilayer Insulations. (LMSC - D349866, Lockheed Missiles and Space Co.; NAS3-14377) NASA CR-134477, 1974.

2. Stochl, Robert J.: Basic Performance of a Multilayer Insulation System Containing 20 to 160 Layers. NASA TN D-7659, 1974.

3. Walburn, A. B.: Development of a Reusable Flightweight Cryogenic Storage System. AIAA Paper 74-726, July 1974.

4. DeWitt, Richard L.; and Boyle, Robert J.: Thermal Performance of an Integrated Thermal Protection System for Long Term Storage of Cryogenic Propellants in Space. NASA TN D-8320, 1976.

5. Miao, David; Barber, James R.; and DeWitt, Richard L.: Design, Fabrication, and Structural Testing of a Lightweight Shadow Shield for Deep Space Application. NASA TN D-8319, 1976.

6. Knoll, Richard H.; and DeWitt, Richard L.: Thermal Performance of a Modularized, Replaceable Multilayer Insulation System for a Cryogenic Stage. NASA TN D-8282, 1976.

7. Carter, J. S.; and Timberlake, T. E.: Filament-Wound, Fiberglass Cryogenic Tank Supports. (BC-8367-FR, Brunswick Corp.; NAS3-14627) NASA CR-120828, 1971.

8. Tien, C. L.; Jagannathan, P. S.; and Chan, C. K.: Lateral Heat Transfer in Cryogenic Multilayer Insulation. Advan. Cryog. Eng., vol. 18, K. D. Timmerhaus, ed., Plenum Press, 1973, pp. 118-123.

9. Burton, K. R.: AMPS Propellant Tank Heat Transfer. GD/CA-584-4-149, General Dynamics/Convair, 1968.

TABLE I. - FLAT-PLATE CALORIMETER TEST RESULTS

Test		Measured heat input, W	Corrections to heat input, W		Net heat input, W	Net MLI heat flux, W/m^2
			Lateral	Null		
[a]1	Null test (no MLI)	0.020	------	-----	0.020	-----
2	Two-blanket MLI	.373	-0.028	0.020	.381	0.388
3	Two-blanket MLI with butt joint	.584	-.006	.020	.570	-----
4	Two-blanket MLI	.473	.010	.020	.443	.452
5	Two-blanket MLI with fiberglass strut	1.260	.039	.235	.986	-----
6	Two-blanket MLI with fiberglass strut[b]	2.410	.072	.235	2.103	-----
7	Null test (with MLI and strut)	.218	-.017	-----	.235	-----
8	Null test (with MLI and strut, copper wires to thermal link removed)	.127	-.022	-----	.149	-----

[a]Previously unpublished data.
[b]Chamber pressure, 6.4×10^{-2} N/m^2.

TABLE II. - PREDICTED BASIC THERMAL PERFORMANCE OF MULTILAYER INSULATION BLANKETS ON FLAT-PLATE CALORIMETER

[Assumed number of shields, 34.]

Test	Assumed MLI conditions			MLI boundary temperature, K		Heat-transfer components			Total predicted heat flux, W/m^2	Total predicted heat input, W
	Layer density, layers/cm	Shield emissivity at room temperature	Interstitial pressure, N/m^2	Hot	Cold	Solid conduction, W/m^2	Radiation, W/m^2	Gaseous conduction, W/m^2		
2	17.4	0.036	7.6×10^{-5}	297.2	32.4	0.177	0.208	0.002	0.387	0.380
4	20.6	.038	1.7×10^{-4}	297.4	47.1	.270	.221	.003	.494	.484
6	20.6	.038	6.4×10^{-2}	293.7	25.7	.268	.208	1.462	1.938	1.902
7	20.6	.038	6.7×10^{-5}	44.3	20.7	.0048	0	.0004	.0052	.0051

TABLE III. - SUMMARY OF HEAT INPUTS FOR TESTS WITH FIBERGLASS STRUT

Test	Measured heat input, W	Corrections, W	Net heat input, W	Heat input, W, through -		Lateral MLI heat input to thermal link, W	Net heat input normal to MLI, W	Total heat input from MLI, W
				Thermal link	Fiberglass strut			
5	1.260	0.274	0.986	0.446	0.140	0.306	0.540	0.846
6	2.410	.307	2.103	.481	.145	.336	1.622	1.958

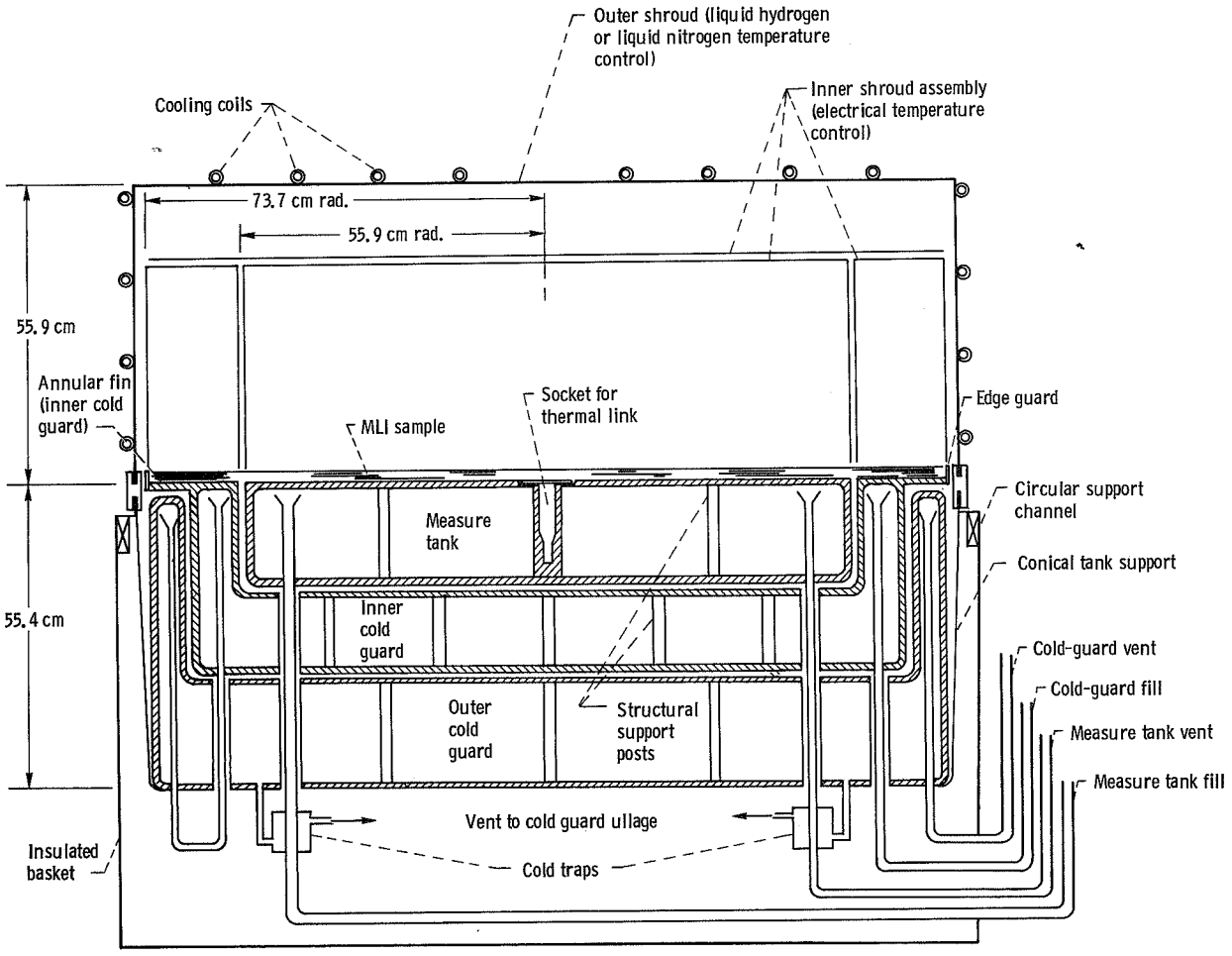

Figure 1. - Cross section of flat-plate calorimeter.

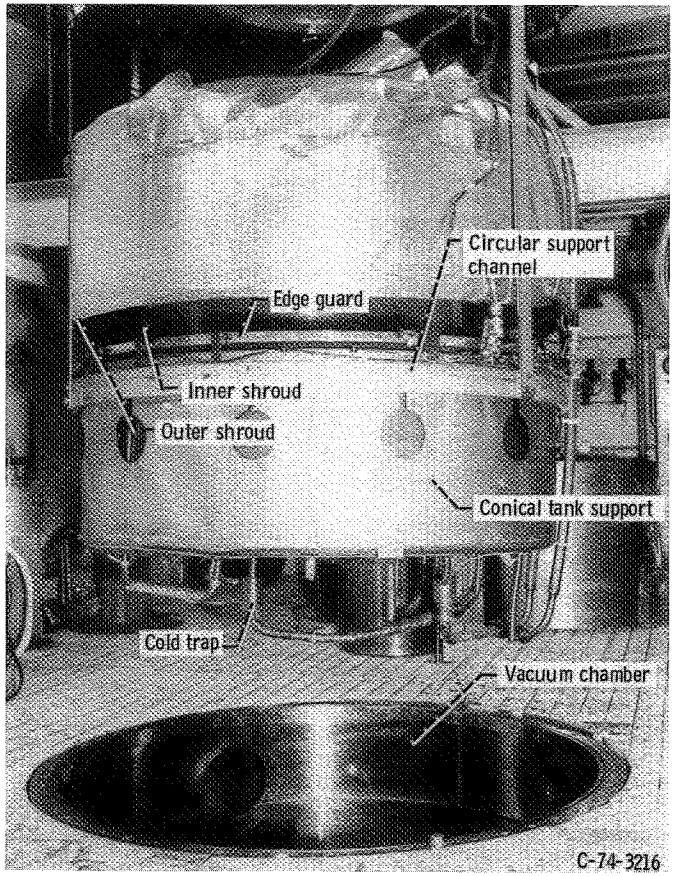

Figure 2. - Calorimeter ready for MLI blanket inspection and installation.

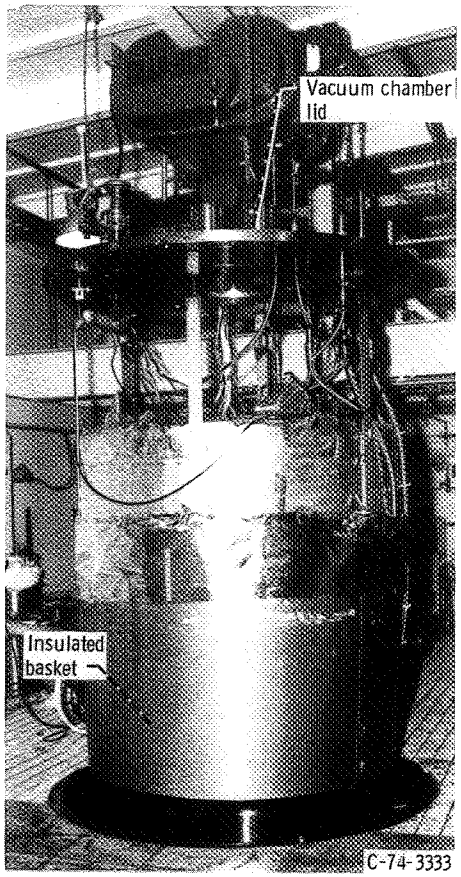

Figure 3. - Calorimeter ready for installation in vacuum chamber.

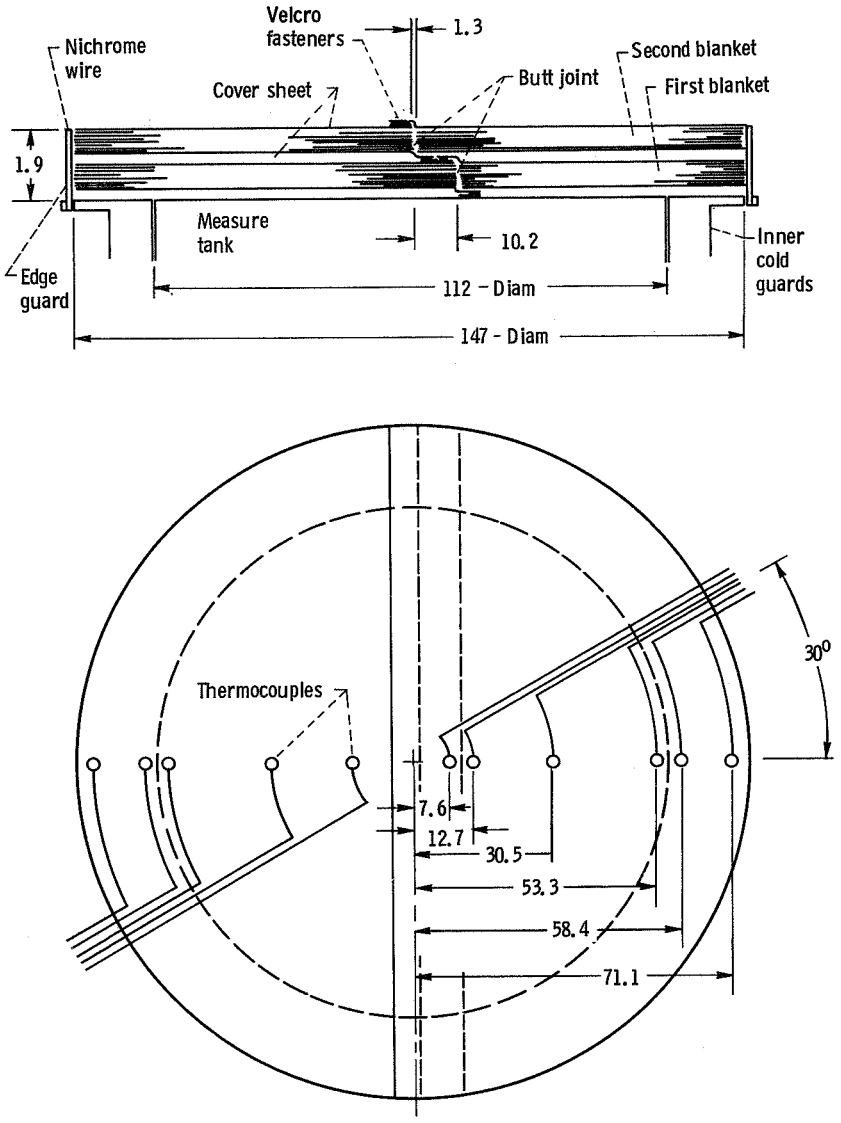

Figure 4. - Butt-joint and radial thermocouple locations for first MLI blanket configuration. NOTE: Radial thermocouple locations are typical of cover sheets (radiation shields 1, 17, 18, and 34) and inner radiation shields 9 and 26. (All dimensions are in cm.)

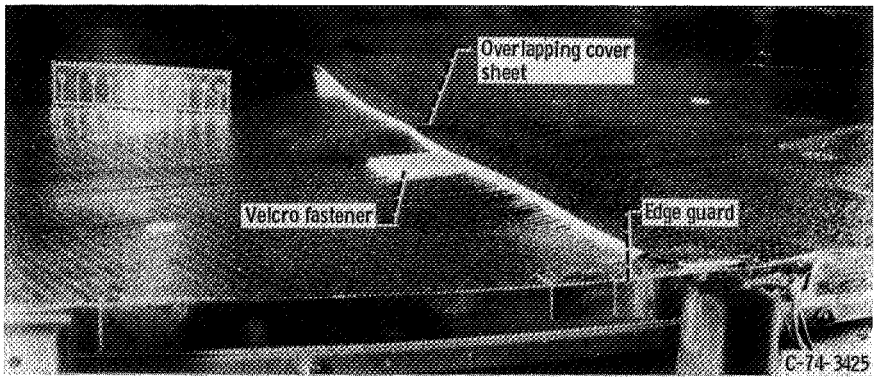

Figure 5. - Installation of MLI blankets with butt joint.

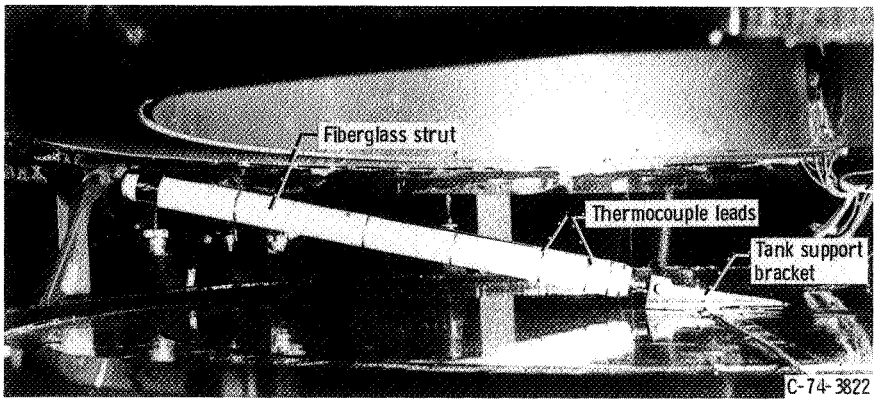

Figure 6. - Installation of fiberglass strut.

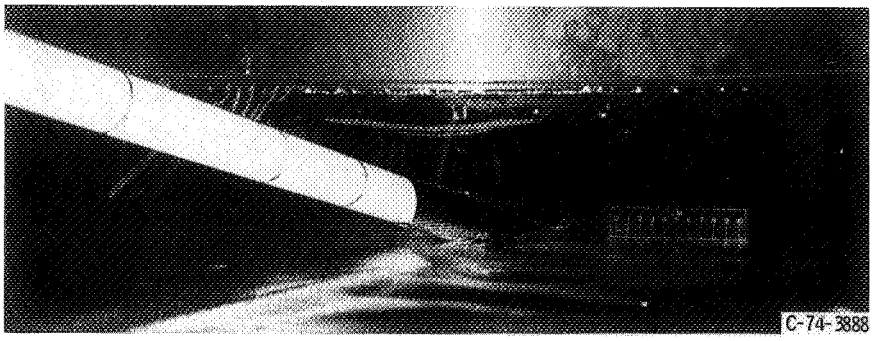

(a) Front view.

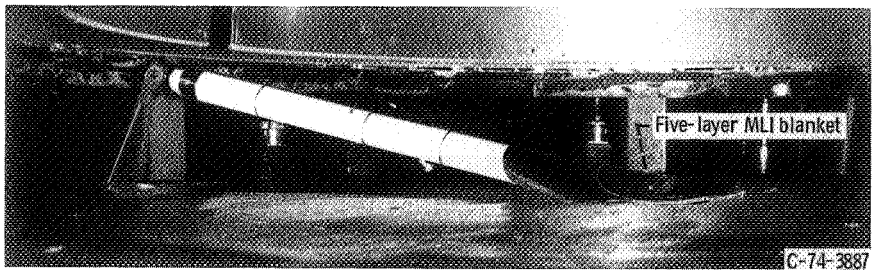

(b) Side view.

Figure 7. - Installation of MLI blankets with fiberglass strut.

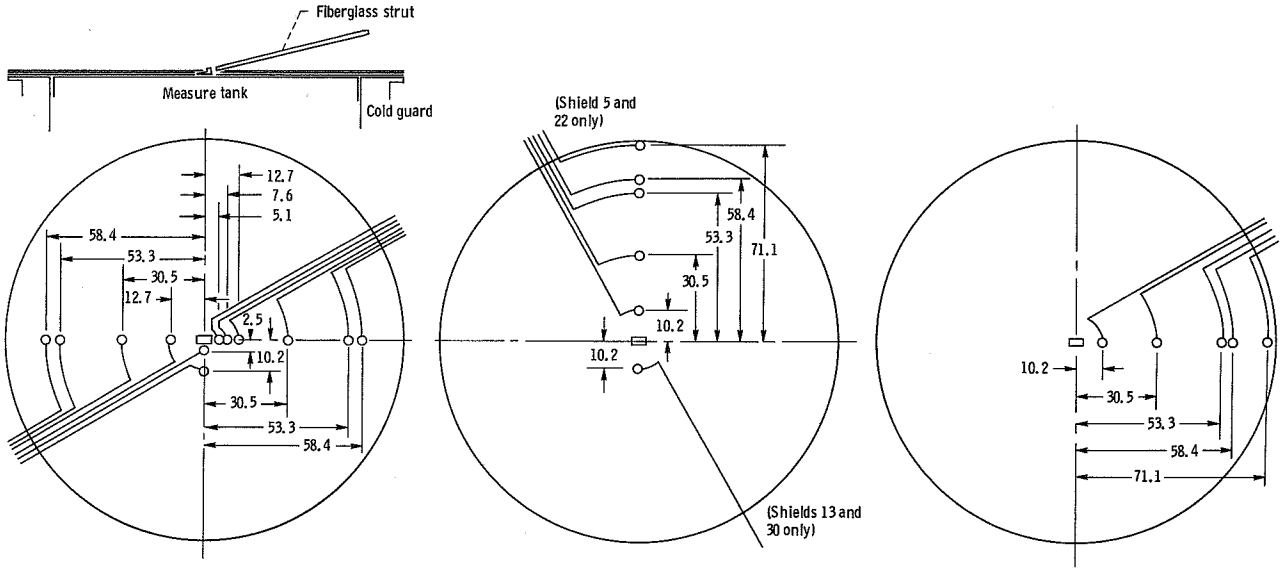

(a) Cover sheets (radiation shields 1, 17, 18, and 34).

(b) Radiation shields 5, 13, 22, and 30.

(c) Radiation shields 9 and 26.

Figure 8. - Thermocouple locations for second MLI blanket configuration. (All dimensions in cm.)

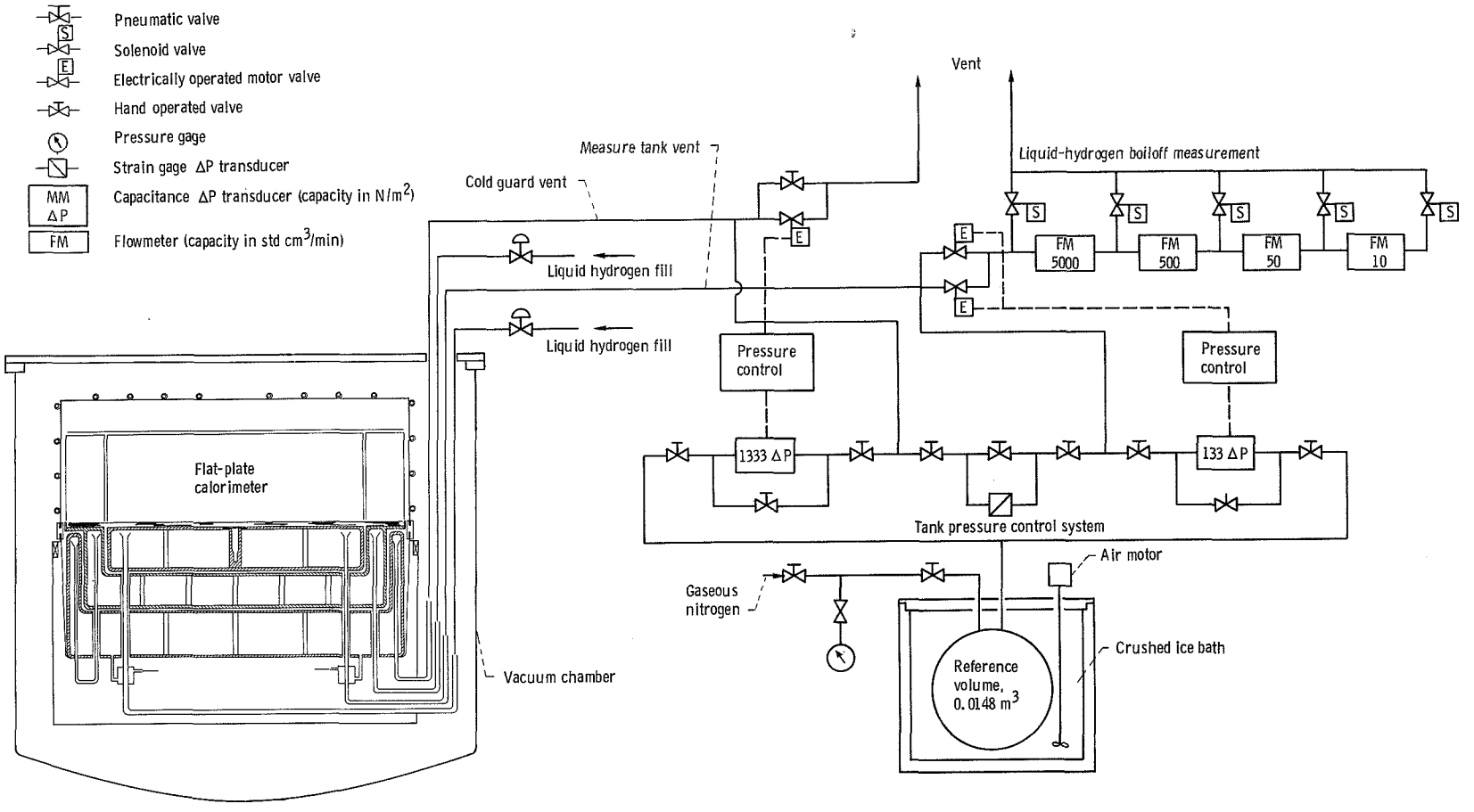

Figure 9. - Facility pressure control and boiloff measurement systems.

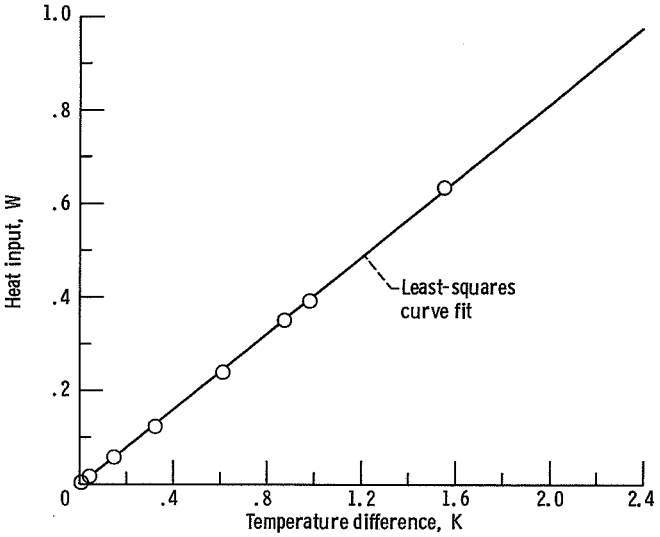

Figure 10. - Thermal-link calibration.

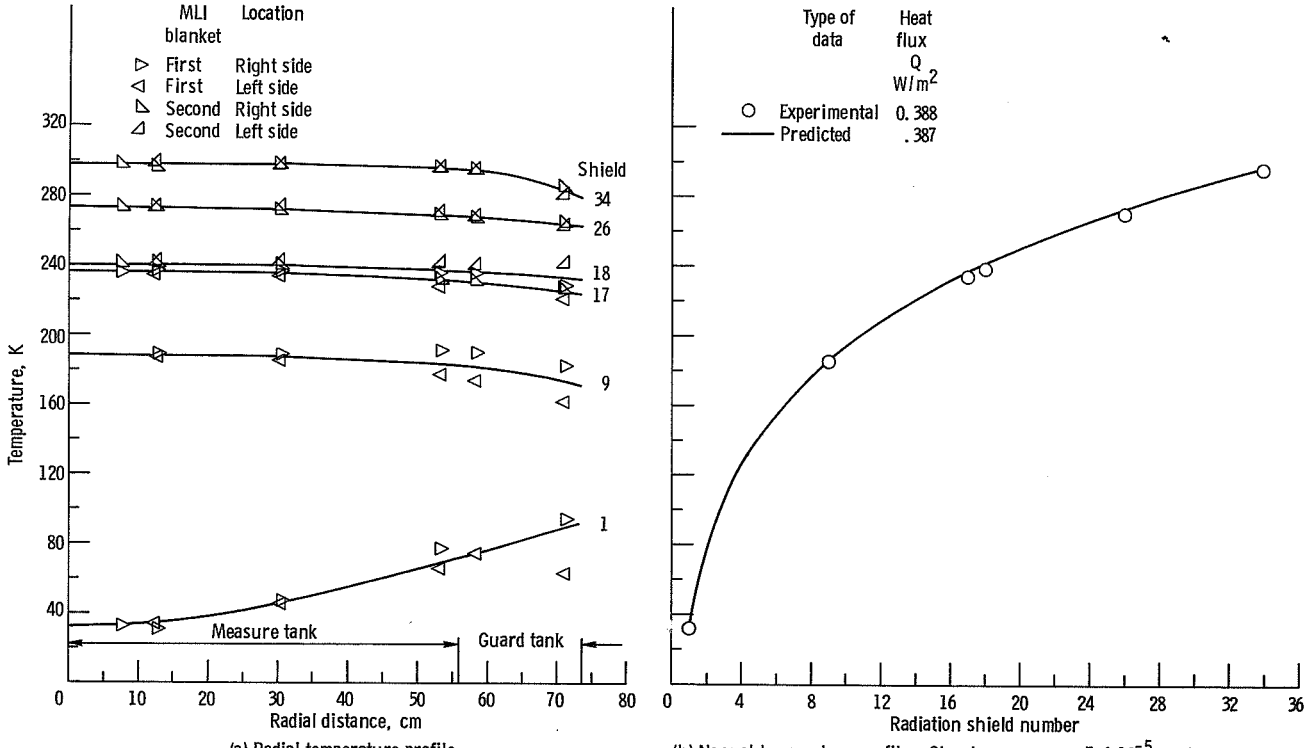

(a) Radial temperature profile.

(b) Normal temperature profile. Chamber pressure, 7.6×10^{-5} newton per square meter; layer density, 17.4; radiation shield emissivity, 0.036.

Figure 11. - MLI temperature profiles for basic thermal performance test; test 2.

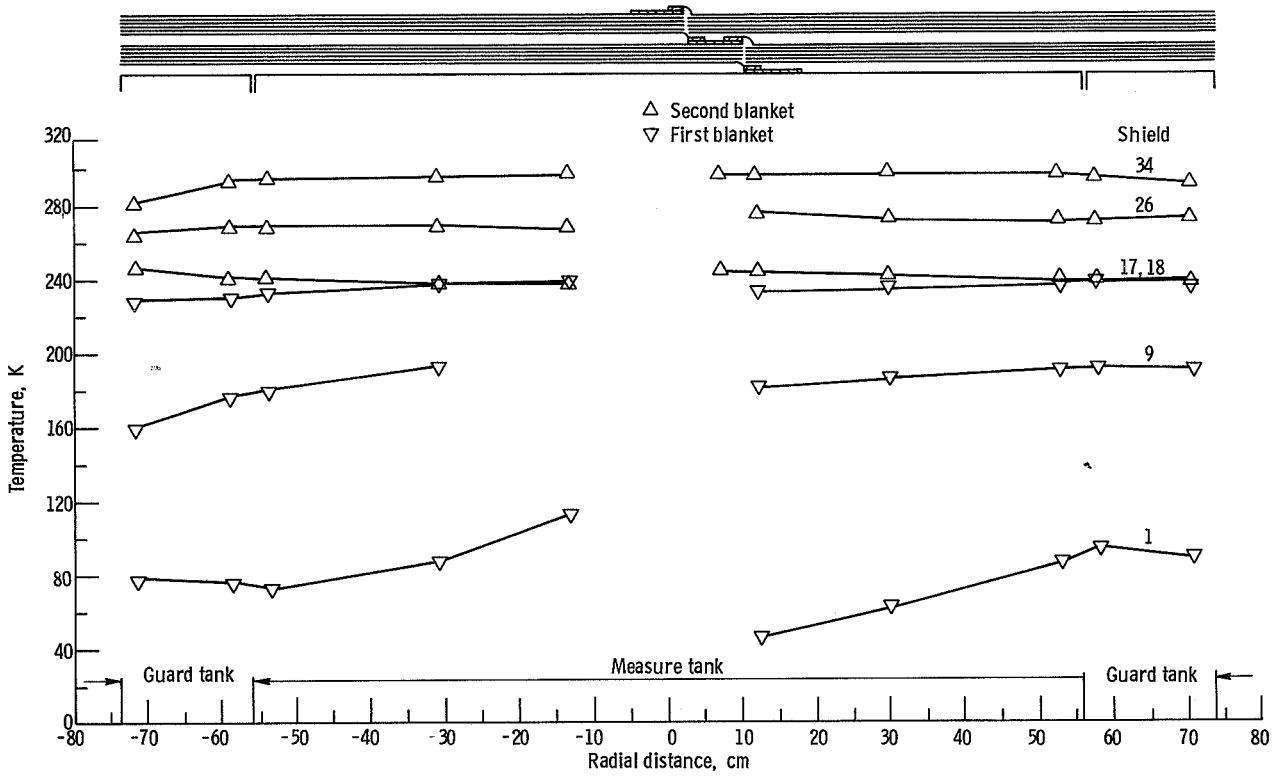

Figure 12. - Radial MLI temperature profile for MLI blankets incorporating butt joint; test 3.

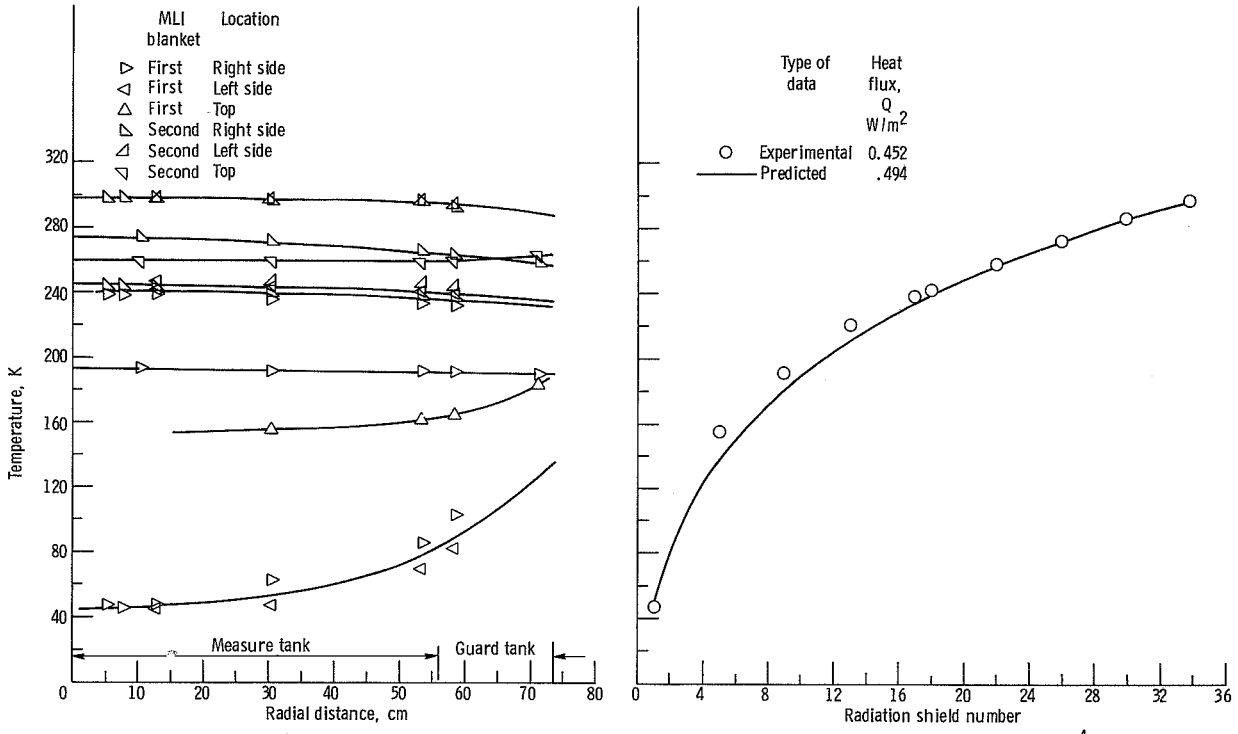

(a) Radial temperature profile.

(b) Normal temperature profile. Chamber pressure, 1.7×10^{-4} newton per square meter; layer density, 20.6; radiation shield emissivity, 0.038.

Figure 13. - MLI temperature profiles for basic thermal performance test; test 4.

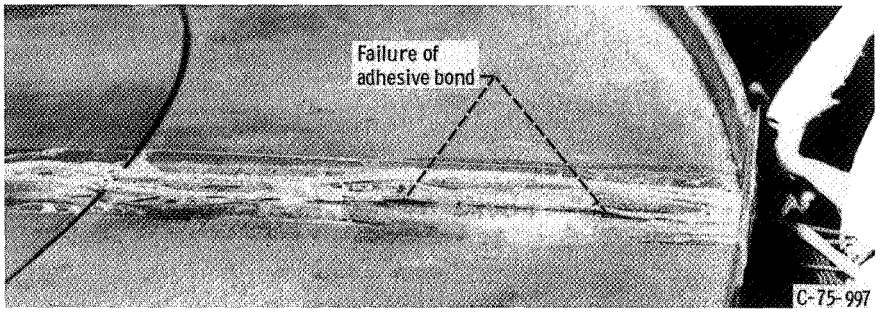

Figure 14. - Area where adhesive bond required to thermally short instrumentation leads to cold guard failed.

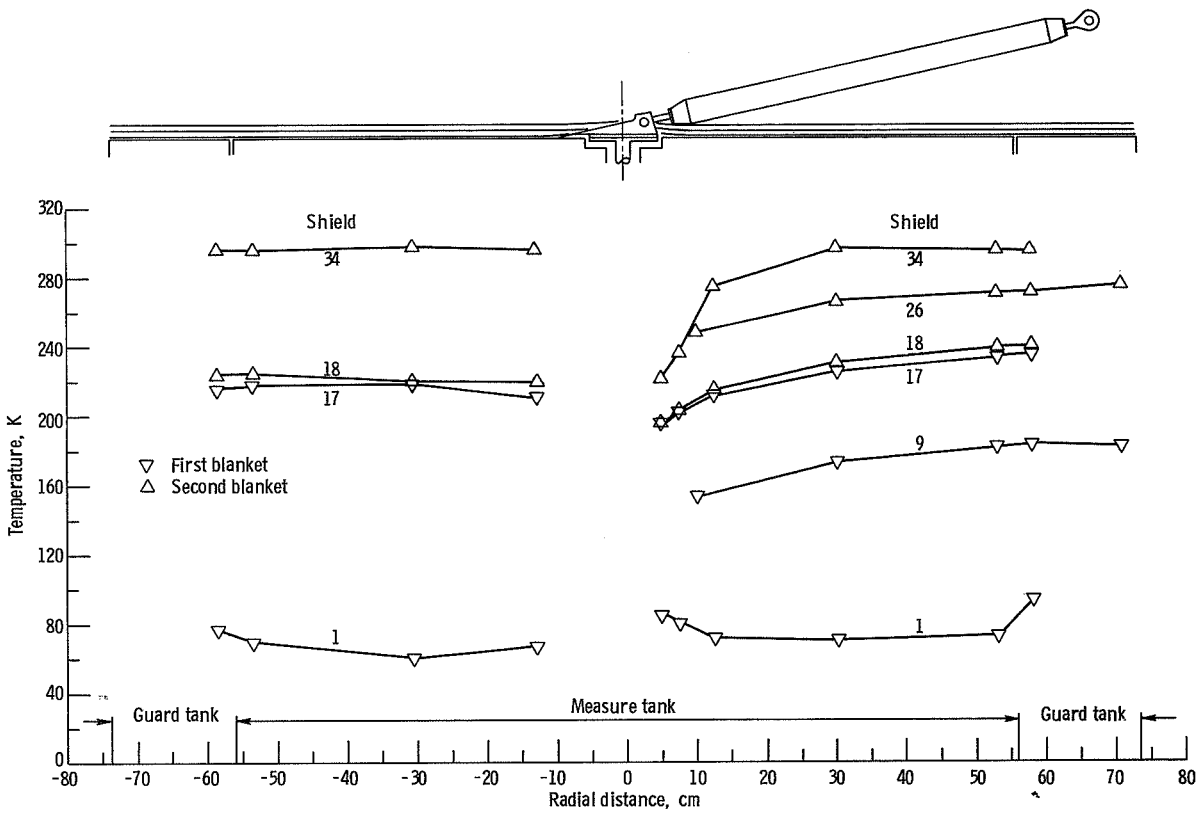

(a) Temperature profile parallel to axis of fiberglass strut.

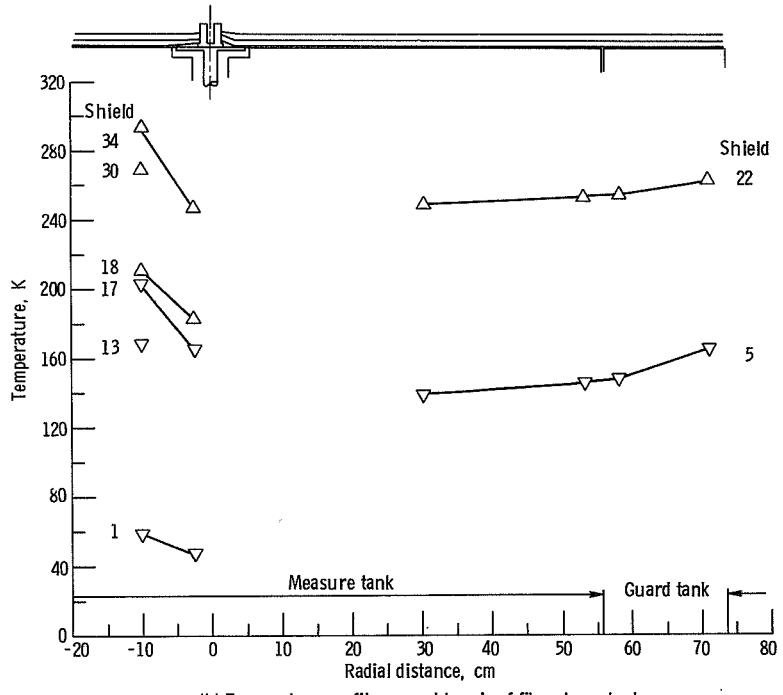

(b) Temperature profile normal to axis of fiberglass strut.

Figure 15. - Radial MLI temperature profile for MLI blankets incorporating penetration; test 5.

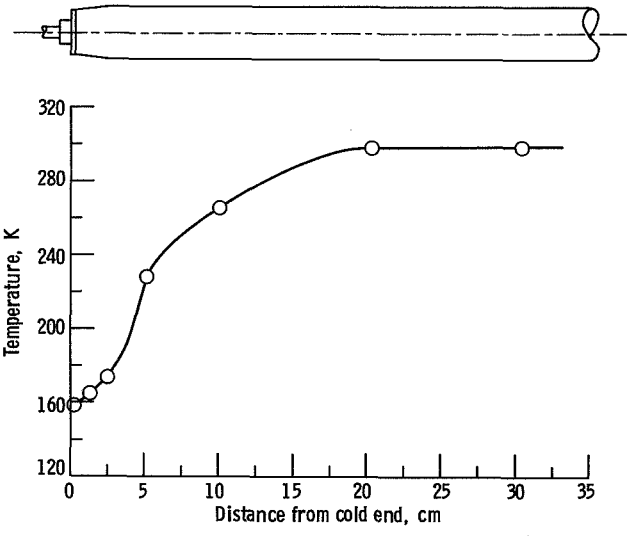

Figure 16. - Temperature profile along fiberglass strut; test 5.

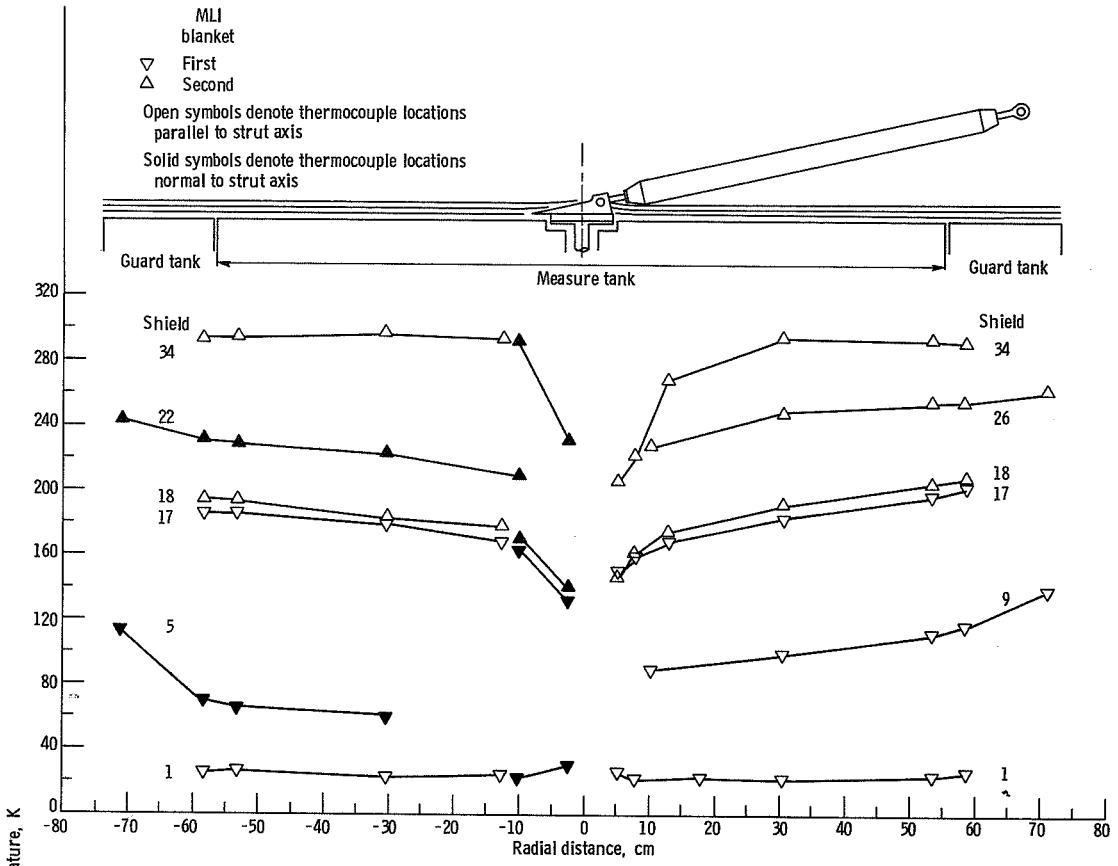

(a) Radial temperature profile.

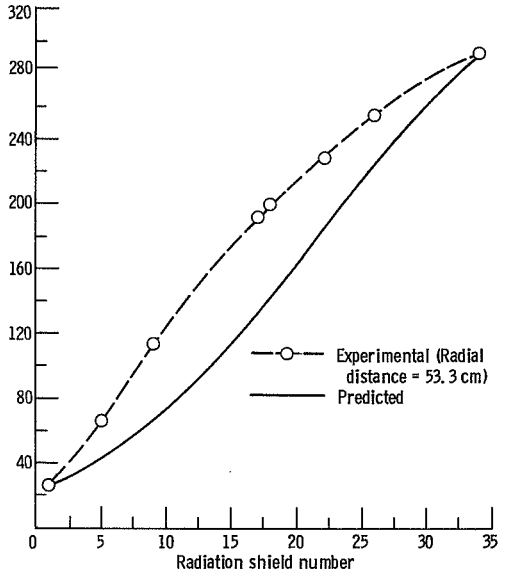

(b) Normal temperature profile. Heat flux, 1.938 watts per square meter; layer density, 20.6 layers per centimeter; radiation shield emissivity, 0.038.

Figure 17. - MLI temperature profile (gaseous helium background) with fiberglass strut. Chamber pressure, 6.4×10^{-2} newton per square meter; test 6.

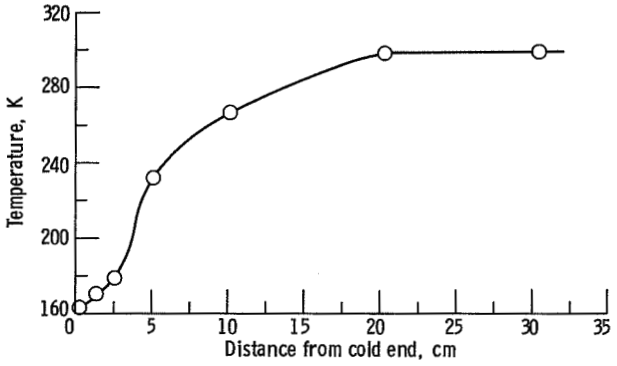

Figure 18. - Temperature profile along fiberglass strut; test 6.

NATIONAL AERONAUTICS AND SPACE ADMINISTRATION
WASHINGTON, D.C. 20546

OFFICIAL BUSINESS
PENALTY FOR PRIVATE USE $300

SPECIAL FOURTH-CLASS RATE BOOK

POSTAGE AND FEES PAID
NATIONAL AERONAUTICS AND SPACE ADMINISTRATION
451

U.S.MAIL

POSTMASTER: If Undeliverable (Section 158 Postal Manual) Do Not Return

"The aeronautical and space activities of the United States shall be conducted so as to contribute . . . to the expansion of human knowledge of phenomena in the atmosphere and space. The Administration shall provide for the widest practicable and appropriate dissemination of information concerning its activities and the results thereof."

—NATIONAL AERONAUTICS AND SPACE ACT OF 1958

NASA SCIENTIFIC AND TECHNICAL PUBLICATIONS

TECHNICAL REPORTS: Scientific and technical information considered important, complete, and a lasting contribution to existing knowledge.

TECHNICAL NOTES: Information less broad in scope but nevertheless of importance as a contribution to existing knowledge.

TECHNICAL MEMORANDUMS: Information receiving limited distribution because of preliminary data, security classification, or other reasons. Also includes conference proceedings with either limited or unlimited distribution.

CONTRACTOR REPORTS: Scientific and technical information generated under a NASA contract or grant and considered an important contribution to existing knowledge.

TECHNICAL TRANSLATIONS: Information published in a foreign language considered to merit NASA distribution in English.

SPECIAL PUBLICATIONS: Information derived from or of value to NASA activities. Publications include final reports of major projects, monographs, data compilations, handbooks, sourcebooks, and special bibliographies.

TECHNOLOGY UTILIZATION PUBLICATIONS: Information on technology used by NASA that may be of particular interest in commercial and other non-aerospace applications. Publications include Tech Briefs, Technology Utilization Reports and Technology Surveys.

Details on the availability of these publications may be obtained from:

SCIENTIFIC AND TECHNICAL INFORMATION OFFICE

NATIONAL AERONAUTICS AND SPACE ADMINISTRATION

Washington, D.C. 20546